Article

Not peer-reviewed version

Temperature-Dependent Luminescence and Defect Recombination Pathways in As-Grown $Gd_3Ga_5O_{12}$ Single Crystals

Gulnara M. Aralbayeva , Zhakyp T. Karipbayev * , Zhalgas T. Abil , Askhat Kakimov , Amangeldy M. Zhunusbekov , Abdirash Akilbekov , Gibrat E. Sagyndykova , Sergii Ubizskii , Kirill Chernenko , Yevheniia Smortsova , Anatolis Sarakovskis , Elena Popova * , Anatolii I. Popov

Posted Date: 29 October 2025

doi: 10.20944/preprints202510.2192.v1

Keywords: $Gd_3Ga_5O_{12}$ single crystals; luminescence; self-trapped excitons (STE); F-centers; defects; thermal quenching; scintillation materials

Article

Temperature-Dependent Luminescence and Defect Recombination Pathways in As-Grown $Gd_3Ga_5O_{12}$ Single Crystals

Gulnara M. Aralbayeva [1], Zhakyp T. Karipbayev [1,*], Zhalgas T. Abil [1], Askhat Kakimov [1], Amangeldy M. Zhunusbekov [1], Abdirash Akilbekov [1], Gibrat E. Sagyndykova [1], Sergii Ubizskii [3], Kirill Chernenko [4], Yevheniia Smortsova [5], Anatolis Sarakovskis [5], Elena Popova [6,*] and Anatoli I. Popov [1,5]

[1] Department of Technical Physics, Institute of Physics and Technology, L.N. Gumilyov Eurasian National University, Satpayev St. 2, Astana 010008, Kazakhstan

[2] Lviv Polytechnic National University, S. Bandera Str. 12, Lviv, 79013, Ukraine

[3] MAX IV Laboratory, Lund University, SE22100, Lund, Sweden

[4] Deutsches Elektronen-Synchrotron (DESY), 22603 Hamburg, Germany

[5] Institute of Solid State Physics, University of Latvia, Kengaraga 8, Street, LV-1063 Riga, Latvia

[6] Department of Physics, University of Maryland, College Park, MD 20742-4111, USA

* Correspondence: Karipbayev_zht_1@enu.kz (Z.T.K.); epopova@umd.edu (E.P.)

Abstract

The intrinsic defect-related luminescence of as-grown $Gd_3Ga_5O_{12}$ (GGG) single crystals was investigated using synchrotron excitation in the vacuum-ultraviolet region. The photoluminescence spectrum at 7 K exhibits a broad emission band centered near ~2.5 eV (≈500 nm), accompanied by narrow 4f–4f transitions of uncontrolled Tb^{3+} impurity ions. Gaussian decomposition of the broad band reveals three components at approximately 3.05, 2.70, and 2.50 eV, attributed to self-trapped excitons (STE), antisite-associated recombination, and F/F^+-type oxygen-vacancy centers, respectively. Temperature-dependent photoluminescence measurements show that the defect-related luminescence is governed by two thermally activated nonradiative channels with activation energies of ~5–8 meV and 42–56 meV. The shallow channel dominates at 20–50 K, while the main quenching occurs between 100 and 150 K, leading to nearly complete suppression of the broad emission at room temperature. The present results therefore characterize the emission behavior of intrinsic, shallow defect centers in as-grown GGG and contribute to understanding defect recombination pathways that are critical for optimizing garnet-based scintillation and photonic materials.

Keywords: $Gd_3Ga_5O_{12}$ single crystals; luminescence; self-trapped excitons (STE); F-centers; defects; thermal quenching; scintillation materials

1. Introduction

Gadolinium gallium garnet ($Gd_3Ga_5O_{12}$, GGG) is a cubic oxide (Ia3d), typically obtained as high-quality single crystals and widely used as a substrate for the epitaxial growth of optical and magneto-optical films [1–4]. Its wide band gap (E_g ≈ 5.6 eV) and high transparency from the infrared to the ultraviolet range determine its value for photonic applications [3]. When doped with rare-earth ions, GGG exhibits efficient phosphor and scintillation behavior: in Ce:GGG, both emission spectra and decay kinetics are governed by the local crystal environment and the chemical nature of the host [5–7], whereas Er^{3+}-, Pr^{3+}-, and Dy^{3+}-doped systems show characteristic f–f transitions [8,9]. For low-temperature phosphor synthesis, sol–gel methods and isomorphic substitutions have been developed [10]. Surface mechanical properties crucial for optical quality have been examined using nanoscratch

 doi:10.20944/preprints202510.2192.v1

and nanoindentation techniques [11–13], and Co diffusion has been identified as a factor influencing color-center formation [14].

In nano- and thin-film forms, the functionality of GGG expands further: GGG:Tb^{3+} and GGG:Eu^{3+} nanoparticles exhibit stable luminescence, including pressure-dependent behavior [15–17], while thin films grown by liquid-phase epitaxy are used in fast scintillators [18,19]. GGG has also been proposed as a wide-band-gap ceramic electrolyte for low-temperature fuel cells [20]. Cr^{3+} doping provides reproducible thermometric characteristics, and Ca/Si cation substitutions in Cr:GGG allow adjustment of emission wavelength and decay time [21,22]. In Ce:GGG, the position of the Ce^{3+} $5d_1$ level relative to the conduction band and shallow traps has been established, which is essential for understanding competition between radiative and trapping channels [23].

GGG is also recognized as a frustrated magnet that exhibits field-induced phase transitions and an enhanced magnetocaloric effect upon Al substitution [24–27]. The crystal demonstrates high radiation resistance: reversible amorphization/recrystallization processes [28], radiation-induced absorption and Raman changes under neutron and heavy-ion irradiation [29–32], and track-formation behavior described by the inelastic thermal spike model have been reported [33–36]. Similarity of radiation response to the garnet matrix in YIG confirms the universality of structural disordering and recovery mechanisms [37,38]. Exceptional mechanical strength and thermal stability of GGG have been verified under dynamic compression up to 2.6 TPa [39].

The intrinsic defect-related luminescence of garnets arises primarily from oxygen-vacancy centers F (V_O with two electrons) and F^+ (V_O with one electron), together with self-trapped and defect-localized excitons (STE/LE). In YAG [43] and LuAG [44], a fast violet emission band at ~3.1–3.2 eV ($\tau \approx 2$–3 ns), excited at ~3.3/5.3/6.5 eV, is attributed to F^+ centers, whereas a blue-green band at ~2.6–2.7 eV corresponds to F centers [43–45]. Antisite disorder (Y_{Al}/Lu_{Al}) promotes the formation of F^+–antisite complexes that shift and broaden these bands and partially suppress STE emission; the F/F^+ centers can also be excited via the excitonic continuum (~6.5–7.3 eV) [43–45].

In GGG-based mixed garnets, such as GAGG:Ce, and in YAG, swift heavy-ion irradiation induces stable photo-induced absorption in the UV–visible range and strongly suppresses VUV-excitonic emission, reflecting increased F-type defect concentrations and competition with Ce^{3+} 5d–4f emission channels, including possible Ce^{3+}/C^{4+} charge conversion [46,47]. For sintered garnet crystals, oxygen partial pressure, grain boundaries, and impurity–defect complexes enhance F/F^+ emission and suppress STE, whereas oxidative annealing reduces color-center populations, which is crucial for optical and scintillation performance. Systematic low-temperature studies of such intrinsic defect-related luminescence in sintered crystals remain scarce, representing a significant open research direction.

However, despite extensive studies of radiation and dopant effects, the native defect structure of as-grown GGG remains insufficiently characterized. Addressing this issue is essential for targeted control of trapping processes, suppression of nonradiative channels, and the rational design of radiation-resistant luminescent materials based on GGG. To fill this gap, in this work we investigate the luminescence and the temperature dependence of luminescence in as-grown GGG.

2. Materials and Methods

$Gd_3Ga_5O_{12}$ (GGG) single crystals were grown by the Czochralski method using an iridium crucible in a weakly oxidizing atmosphere at the SRC "Electron-Carat" (Lviv, Ukraine) [33]. The growth atmosphere consisted of a mixture of 98% Ar and 2% O_2. High-purity oxides Gd_2O_3 and Ga_2O_3 (99.99 wt%) were used as starting materials. It is known that the presence of tetravalent impurity ions (such as Si^{4+} and Zr^{4+}) in the starting oxides can lead to the formation of cation vacancies and promote a spiral growth mechanism in rare-earth gallium garnet crystals. To suppress these effects, a small amount (10^{-2}–10^{-3} wt.%) of calcium oxide (CaO) was added to the melt.

It should also be noted that GGG crystals usually contain a small amount (10^{-3}–10^{-4} wt.%) of uncontrolled impurity ions, which is practically unavoidable during the growth process. The samples

 doi:10.20944/preprints202510.2192.v1

were prepared in the form of flat plates with a thickness of 0.48 mm, oriented along the (111) plane, and polished on both sides to optical quality.

Luminescence spectroscopy measurements were performed under synchrotron radiation excitation. The excitation and emission spectra were recorded at the FinEstBeAMS undulator beamline [48–54], located at the 1.5 GeV storage ring of the MAX IV synchrotron facility (Lund, Sweden). The excitation photon energy range extended from 4.5 to 11.0 eV. Emission in the UV–visible region (200–700 nm) was analyzed using an Andor Shamrock SR-303i (0.3 m) monochromator coupled to a Newton DU970P-BVF CCD detector, providing a total detection range of 200–900 nm. The GGG samples were mounted on the cold finger of a closed-cycle cryostat (Advanced Research Systems) and positioned inside an ultra-high-vacuum chamber maintained at a pressure of ~10^{-9} mbar.

Luminescence was studied at 9 K using synchrotron radiation at the Superlumi P66 beamline (PETRA III, DESY) [55]. Excitation was selected by a 2 m monochromator with a spectral resolution of 4 Å. The emitted luminescence was analyzed using an ANDOR Kymera monochromator (2 Å resolution) equipped with a CCD camera and a Hamamatsu R6358 photomultiplier. The excitation spectra were corrected using a sodium salicylate standard to ensure data accuracy.

3. Results and Discussion

The absorption spectrum exhibits a steep increase in absorption at $\lambda \lesssim 225$ nm (≈5.6–5.7 eV), corresponding to the fundamental band-gap edge of GGG [3]. In the UV–visible region, three weak bands are observed at 254, 275, and 313 nm, assigned to intra-configurational transitions of Gd^{3+}: $^8S_{7/2} \rightarrow {}^6D_j$ (254 nm), $^8S_{7/2} \rightarrow {}^6I_j$ (275 nm), and $^8S_{7/2} \rightarrow {}^6P_j$ (313 nm). The presence of Ca^{2+} (introduced as a charge-compensating additive) manifests as an additional weak band near ≈350 nm (≈3.55 eV) [30,33].

The photoluminescence spectra under pulsed-laser excitation at $\lambda_{ex} = 230$ nm (≈5.4 eV), i.e., near the Gd–O charge-transfer edge and effectively pumping both host and defect centers, were measured at T = 7 K. The spectrum spans 3.3–1.8 eV (375–688 nm) and consists of (i) a broad defect-related band with a maximum at ≈475 nm, attributed to recombination involving oxygen-vacancy-related centers, including F-type centers and antisite-associated defects, and (ii) narrow Tb^{3+} lines at 382, 420, 440, 474, 543, 583, and 630 nm, corresponding to $^5D_3/^5D_4 \rightarrow {}^7F_j$ transitions (see Table 1) [16, 87].

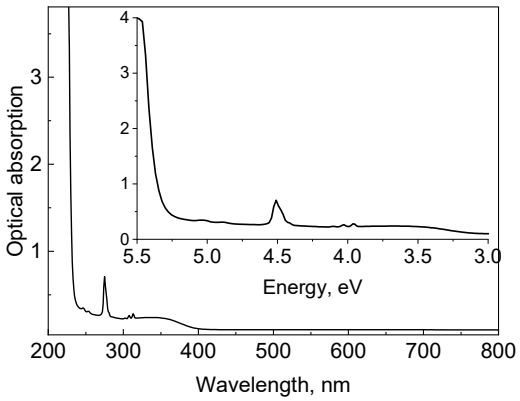

Figure 1. Absorption spectra of GGG.

 doi:10.20944/preprints202510.2192.v1

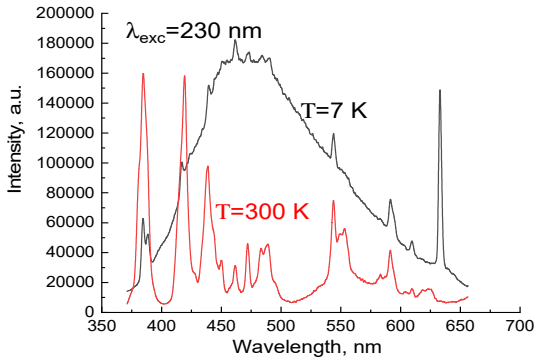

Figure 2. Luminescence spectra of GGG at 7 and 300 K.

Gaussian decomposition of the broad band reveals three subcomponents centered at 3.05, 2.70, and 2.50 eV. By analogy with related garnets such as YAG and LuAG [43,44,56], the 2.50 eV component is associated with F-center recombination, whereas the 3.05 and 2.70 eV components are likely due to STE emission and radiative recombination near Gd_{Ga} antisite environments. At 300 K, the defect-related band is almost entirely quenched, while the narrow Tb^{3+} emission persists, with the $^5D_4 \rightarrow {}^7F_5$ transition at 543 nm being the most thermally stable. The fact that the defect emission disappears at approximately 300 K suggests that at room temperature, non-radiative processes (probably thermally activated release of charge carriers from traps or transition to the non-radiative recombination pathway) predominate over radiative recombination for these defect centers.

Table 1. Main luminescence peaks of Tb^{3+} ions and transitions in GGG single crystal

Emission Band, (nm)	Excitation, (nm)	Possible Transitions
382	230	$^5D_3 \rightarrow {}^7F_6$
420	230	$^5D_3 \rightarrow {}^7F_5$
440	230	$^5D_3 \rightarrow {}^7F_4$
474	230	$^5D_4 \rightarrow {}^7F_6$
543	230	$^5D_4 \rightarrow {}^7F_5$
583	230	$^5D_4 \rightarrow {}^7F_4$
630	230	$^5D_4 \rightarrow {}^7F_3$

Figure 3a presents the VUV excitation spectrum of the GGG crystal measured at 7 K (monitoring the broad emission band across the full range). The spectrum is dominated by a very intense, broad excitation band spanning approximately 4.5–5.8 eV. The presence and strength of this feature indicate a high concentration of defect-related states introduced during crystal growth.

Within this broad 4.5–5.8 eV band, at least three sub-bands can be distinguished. Multi-peak Gaussian decomposition (Figure 3b) reveals maxima at approximately 4.9, 5.3, and 5.5 eV. Each component may be attributed to a specific electronic transition. The highest-energy component (~5.5 eV) corresponds to the intrinsic charge-transfer band of the GGG lattice. In rare-earth garnets, charge-transfer (CT) transitions typically involve electron transfer from O 2p states either into the conduction band or directly to a rare-earth ion [41]. The fundamental absorption edge of GGG lies at ~5.6–5.7 eV [3], therefore the 5.5 eV band likely corresponds to excitation across the band gap or to a bound exciton just below the conduction band. This feature reflects host-lattice excitation, which subsequently relaxes and emits via defect- or matrix-related channels. Its broad character, rather than a sharp line, is consistent with an extended, delocalized excitation.

 doi:10.20944/preprints202510.2192.v1

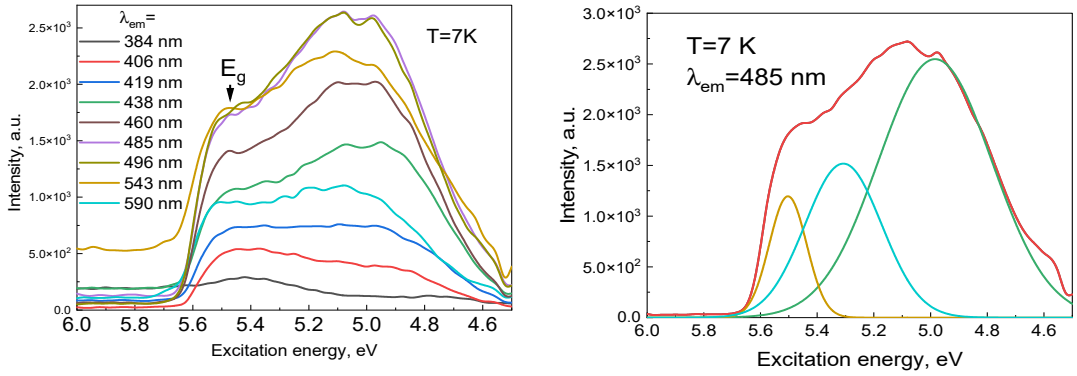

(**a**) (**b**)

Figure 3. Excitation spectrum of GGG luminescence at 7 K **(a)** and Gaussian deconvolution of the spectrum at 485 nm **(b)**.

The intermediate sub-band (~5.3 eV) is associated with oxygen-vacancy-related states and/or self-trapped excitons (STE). Oxygen vacancies in GGG (F-centers when capturing an electron) produce in-gap states that can be excited in this energy range. In the related mixed garnet $Gd_3Al_2Ga_3O_{12}$:Ce (GAGG:Ce), an excitation band at 5.2–5.3 eV under VUV irradiation has been assigned to STE localized at anion vacancies, eventually leading to F-center formation [40,46]. Thus, we attribute the 5.3 eV band in GGG to excitation of STE or vacancy-associated intermediate states, which may either decay radiatively or convert into stable F-centers.

The lowest-energy excitation component (~4.9 eV, with a shoulder down to ~4.7 eV) corresponds to deeper defect states. These may involve antisite defects or more complex vacancy clusters. Gd/Ga antisite defects (Gd^{3+} on a Ga site) introduce strongly localized electronic states due to the altered crystal field and charge-compensation environment. Such antisites can capture excitons or charge carriers. Therefore, the 4.9 eV band likely corresponds to excitons bound to Gd_{Ga} antisites or vacancy–defect complexes. The lower excitation energy indicates that these states lie relatively deep within the band gap.

Notably, pristine GGG already exhibits a rich defect-excitation structure. Previous studies of GGG irradiated with heavy ions or neutrons also reported the formation of color centers producing new absorption and luminescence bands [30,32,33]. Potera et al. showed that electron-irradiated GGG develops transient absorption bands near 5.0 eV and 4.3 eV, attributed to F^+ and F centers, respectively [31]. These absorptions correspond to excitation of the same defect centers observed here in luminescence.

Thus, the excitation spectrum (Figure 4) provides the first direct insight into the nature and energetic hierarchy of luminescent defect states in GGG.

The luminescence spectrum at 7 K was further analyzed using a Gaussian decomposition to resolve overlapping components (Figure 4). In this figure, the broad 477 nm band (excited at 230 nm) was decomposed into several Gaussian subbands, excluding the narrow Tb^3+ lines, which were selected separately or removed for clarity. The analysis revealed three main broadband components with peak positions approximately at 400 nm, 467 nm, and 507 nm (in terms of photon energy, this corresponds to ~3.1 eV, ~2.65 eV, and ~2.45 eV, respectively). These values closely match the subband energies deduced from the excitation spectrum analysis earlier (3.05 eV, 2.70 eV, 2.50 eV). Each subband likely corresponds to a different type of defect center recombination. The 507 nm component (2.45–2.50 eV) is attributed to F-centers. In the classical model, an F-center can trap a hole (forming an excited state F) and then emit a photon upon relaxation to the ground state. Andriychuk et al. observed broad luminescence with a wavelength of 2.5 eV in GGG and attributed it to such recombination of radiation-induced color centers [56]. Our results are consistent with this: the 507 nm band appears in the unirradiated crystal (which likely contains some intrinsic oxygen vacancies from growth). Our data convincingly show that the key effect of defective optics of GGG is the broad

 doi:10.20944/preprints202510.2192.v1

band at ~500 nm (≈2.5 eV): its amplitude is maximum at 7 K, and at 300 K it almost completely disappears while narrow Tb^{3+} lines are preserved, confirming its matrix-defect nature and excluding the contribution of 4f–4f transitions. Gaussian deconvolution isolates the contribution at 2.50 eV as a signal of F/F^+ centers (oxygen vacancies), while the neighboring subbands at 2.70 and 3.05 eV are associated with STE and antisites; together with edge pumping at 230 nm (≈5.4 eV) [33,56]. In support of this, we present the results of a study where, in epitaxial GGG films grown from a Bi_2O_3–B_2O_3 solution-melt, the authors attribute a broad luminescence band with a maximum at about 500 nm to Bi^{3+} ions [57]. This emission, observed with selective ultraviolet synchrotron excitation, manifests itself as a broad band in the range of 380–750 nm. It is important to note that the authors report strong luminescence at room temperature (300 K), the intensity of which decreases by only 20% upon heating from 10 K. This distinguishes their results from our samples, in which the broad glow at room temperature is quenched.

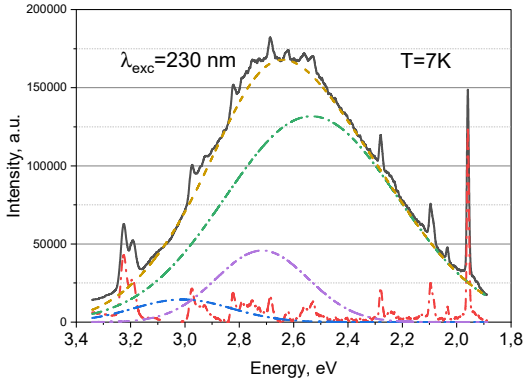

Figure 4. Luminescence spectrum of GGG at 7 K with Gaussian deconvolution (λ_{ex} = 230 nm).

The temperature dependence of luminescence intensity for GGG crystal (Figure 4) was investigated. Thermal quenching of luminescence bands associated with defect centers is often analyzed using the empirical expression (Table 1):

$$I = \frac{I_0}{\left(1 + \sum_i B_i \, e^{-\frac{E_i}{k_B T}}\right)} \quad (1)$$

Where I_0 is the photoluminescence intensity at very low temperature, B_i are constants, and E_i are the activation energies of nonradiative levels. The physical meaning of B_i depends on the adopted model of thermal quenching. The calculated activation energies are summarized in Table 2.

For all four emission bands centered at 406, 467, 507, and 550 nm, an initial decrease in intensity is observed with increasing temperature. This behavior is governed by a shallow activation channel with E_1 = 5–8 meV and B_1 = 3.65–11.5. The characteristic onset temperature $T_{on} \approx E_1/[k_B \ln B_1]$ is found to be 31–35 K for the 467 and 507 nm bands and ~46–54 K for the 406 and 550 nm bands. This regime corresponds to thermal release of carriers from very shallow localized states within the defect complex, leading to a redistribution between radiative and nonradiative pathways even at cryogenic temperatures.

The dominant contribution originates from a second channel with activation energies E_2 = 41.7–55.6 meV and large pre-exponential factors B_2 = 50–615. The temperature of half-quenching, defined by $I(T_{1/2}) = I_0/2$, is estimated as $T_{1/2} \approx E_2/[k_B \ln B_2]$). For the 507 and 467 nm bands, $T_{1/2} \approx 100-103$ K; for the 406 and 550 nm bands, $T_{1/2} \approx 123-124$ K. These values are in full agreement with the experimental trends shown in Figure 4b, where the intensity decays by approximately one order of magnitude between 80 and 150 K and approaches the noise level above 150 K.

The 467 and 507 nm bands exhibit nearly identical activation parameters ($E_2 \approx 55.6$ meV, large B_2), indicating a common origin associated with recombination involving oxygen vacancies in F/F^+ configurations. In contrast, the 406 and 550 nm bands, characterized by slightly lower activation

 doi:10.20944/preprints202510.2192.v1

energies $E_2 \approx 41.7-41.8$ meV and significantly smaller B_2, reflect contributions from defects which possess a weaker temperature sensitivity and persist to slightly higher temperatures.

Unlike the defect-related broad bands, the sharp 4f–4f transitions of Tb^{3+} remain observable at 300 K due to strong shielding of the 4f electrons, confirming that the broad emission is not impurity-derived but arises from matrix intrinsic defects.

The temperature dependence of photoluminescence quantitatively demonstrates that defect-related emission in GGG is governed by the competition between a shallow activation channel (5–8 meV) dominating at 20–50 K and a main nonradiative channel with activation energy of 42–56 meV, which controls the quenching between 100 and 150 K. The derived activation energies and intensity trends are consistent with recombination processes involving oxygen-vacancy-related centers (F/F^+) and associated defect complexes [31,56], explaining the disappearance of the broad emission band near 500 nm at room temperature while the Tb^{3+} lines remain unaffected.

In contrast to our non-irradiated GGG crystal, where the defect-related emission band near 2.5 eV (≈500 nm) is fully quenched by ~300 K due to shallow activation energies (~42–56 meV), strongly X-ray–irradiated GGG (GGG-V) reported by Andriichuk *et al.* [56] retains the same emission to temperatures above 500 K. In those irradiated samples, the excitation spectrum contains two pronounced bands at 4.5 and 5.44 eV, and distinct TSL and thermally stimulated electron emission peaks appear in the range 145–285 K, indicating the formation of deeper and thermally stable oxygen-vacancy–related trap complexes. Thus, our results represent the behavior of as sintered, shallow defect centers, whereas the literature data reflect radiation-induced stabilization of deeper vacancy aggregates.

Table 2. Obtained by Eq(1) activation energy values of defect centers in GGG single crystal.

λ_{em}, nm	B_1	E_1, meV	B_2	E_2, meV
406	3,65	6	50,3	41,7
467	7.9	5.6	521	55.6
507	11.5	7.3	614.9	55.6
550	5,95	6,2	51,7	41,8

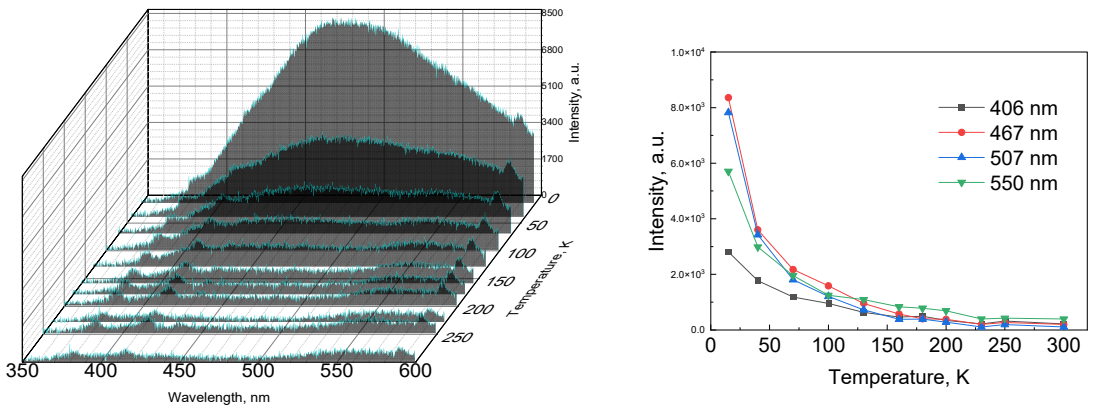

(**a**) (**b**)

Figure 4. Temperature dependence of the luminescence spectra GGG single crystal (a) and temperature dependence on several bands (b).

4. Conclusions

In this work, we have established the optical signatures and thermal stability of defect-related luminescence in as-grown GGG single crystals. Low-temperature photoluminescence spectra reveal a broad emission band centered near ~2.5 eV (~500 nm), accompanied by characteristic 4f–4f

 doi:10.20944/preprints202510.2192.v1

transitions of residual Tb^{3+} ions. Spectral deconvolution demonstrated that the broad band consists of three contributions located at ~3.05, 2.70, and 2.50 eV, which were assigned to self-trapped exciton recombination, antisite-defect–assisted emission, and oxygen-vacancy centers (F/F^+), respectively.

The temperature dependence of the luminescence intensity showed that the defect-related emission is controlled by two thermally activated nonradiative channels with activation energies of ~5–8 meV and 42–56 meV. The main quenching occurs between 100 and 150 K, leading to the near-complete disappearance of the broad emission at room temperature. This behavior confirms that shallow vacancy-related centers dominate the recombination processes in the as-grown material.

Comparison with previously reported X-ray–irradiated GGG demonstrated a notable difference in trap depth and thermal stability: while irradiated crystals retain 2.5 eV emission up to >500 K, the emission in our samples is fully quenched by ~300 K. Thus, the present study characterizes the luminescence behavior of native defect complexes and provides quantitative insight into their recombination and thermal deactivation mechanisms, relevant for the optimization of garnet-based scintillators and optical ceramics.

Author Contributions: Conceptualization, G.M.A., Z.T.K., A.Ki. and S.U.; methodology, Z.T.K. and A.Ki.; software, G.E.S. and E.P.; validation, Z.T.A., E.P., S.U. and A.Sa.; formal analysis, Z.T.A., A.Ka., A.Ki., G.E.S. and Y.Sm.; investigation, Z.T.A., A.Ka., A.M.Zh., G.E.S., S.U. and A.Sa.; resources, A.Ka., A.M.Zh., S.U., K.Ch., Y.Sm. and A.I.P.; data curation, G.M.A., Z.T.K., Z.T.A., A.Ka., A.M.Zh., E.P., K.Ch., Y.Sm. and A.Sa.; writing—original draft preparation, Z.T.K.; writing—review and editing, G.M.A., Z.T.K. and A.I.P.; visualization, Z.T.A., A.M.Zh., G.E.S., E.P., K.Ch. and Y.Sm.; supervision, A.Ki. and A.I.P.; project administration, G.M.A. and A.I.P.; funding acquisition, G.M.A.

Funding: This research was funded by the Science Committee of the Ministry of Science and Higher Education of the Republic of Kazakhstan (grant number AP19680626). In addition, Anatoli I. Popov was supported by Latvian research project lzp-2023/1-0453 “Prediction of long-term stability of functional materials under extreme radiation conditions” and the Latvian State Research Program No. VPP-IZM-CERN-2022/1-0001.

Data Availability Statement: The raw data supporting the conclusions of this article will be made available by the authors upon reasonable request.

Acknowledgments: The authors MAX IV Laboratory for time on FinEstBeAMS Beamline under Proposal 20231736. The authors acknowledge DESY (Hamburg, Germany), a member of the Helmholtz Association HGF, for providing experimental facilities. The work was carried out at the P66 beamline of PETRA III. Beamtime was allocated under proposal I-20231138.

Conflicts of Interest: The authors declare no conflict of interest.

References

1. O’Kane, D.F.; Sadagopan, V.; Geiss, E.A.; Mandel, E. Crystal Growth and Characterization of Gadolinium Gallium Garnet. J. Electrochem. Soc. 1973, 120, 1272–1278.
2. Xu, Y.-N.; Ching, W.Y.; Brickeen, B.K. Electronic structure and bonding in garnet crystals Electronic structure and bonding in garnet crystals Gd3Sc2Ga3O12, Gd3Sc2Al3O12, and Gd3Ga3O12 compared to Y3Al3O12. Phys. Rev. B 2000, 61, 1817.
3. Ghimire, K.; Haneef, H.F.; Collins, R.W.; Podraza, N.J. Optical Properties of Single-Crystal $Gd_3Ga_5O_{12}$ from the Infrared to the Ultraviolet. Phys. Status Solidi B 2015, 252, 2191–2198.
4. Zhao, G.; Li, T.; Xu, J. Growth of epitaxial substrate Gd3Ga3O12 (GGG) single crystal through pure GGG phase polycrystalline material. J. Cryst. Growth 2002, 237-239, 720–724.
5. Syvorotka, I.I.; Sugak, D.Y.; Wierzbicka, A.; Wittlin, A.; Przybylińska, H.; Barzowska, J.; Barcz, A.J.; Berkowski, M.; Domagała, J.Z.; Mahlik, S.; et al. Optical Properties of Pure and Ce^{3+}-Doped Gadolinium Gallium Garnet Crystals and Epitaxial Layers. J. Lumin. 2015, 164, 31–37. https://doi.org/10.1016/j.jlumin.2015.03.014

 doi:10.20944/preprints202510.2192.v1

6. Mikhailov, M.M.; Neshchimenko, V.V.; Shavlyuk, V.V. Binding-Type Effects in LED Phosphor GGG:Ce^{3+}. Opt. Mater. 2014, 38, 33–36.
7. Thirumalaisamy, T.K.; Saravanakumar, S.; Butkute, S.; Kareiva, A.; Saravanan, R. Structure and Charge Density of Ce-Doped GGG. J. Mater. Sci. Mater. Electron. 2016, 27, 1920–1928.
8. Wang, Y.; You, Z.; Li, J.; Zhu, Z.; Ma, E.; Tu, C. Spectroscopy of Highly Doped Er^{3+}:GGG and Er^{3+}/Pr^{3+}:GGG. J. Phys. D: Appl. Phys. 2009, 42, 215406.
9. Wang, Y.; You, Z.; Li, J.; Zhu, Z.; Tu, C. Optical Properties of Dy^{3+} in GGG. J. Phys. D: Appl. Phys. 2010, 43, 075402.
10. Butkute, S.; Zabiliute, A.; Skaudzius, R.; Zukauskas, A.; Kareiva, A. Sol–Gel Synthesis and Substitution in Ga-Garnets. J. Sol-Gel Sci. Technol. 2015, 76, 210–219.
11. Li, C.; Zhang, F.; Meng, B.; Rao, X.; Zhou, Y. Varied-Depth Nanoscratch on GGG. Mater. Des. 2017, 125, 180–188.
12. Li, C.; Wu, Y.; Li, X.; Ma, L.; Zhang, F.; Huang, H. Nanoindentation of GGG Single Crystal. Appl. Opt. 2018, 57, 3661–3668.
13. Li, C.; Zhang, F.; Wang, X.; Rao, X. Crack-Free Grinding of GGG. J. Mater. Process. Technol. 2020, 279, 116577.
14. Sugak, D.; Syvorotka, I.I.; Yakhnevych, U.; Buryy, O.; Vakiv, M.; Ubizskii, S.; Włodarczyk, D.; 3hydachevskyy, Ya.; Pieniążek, A.; Jakiela, R.; Suchocki, A. Investigation of Co Ions Diffusion in $Gd_3Ga_5O_{12}$ Single Crystals. Acta Phys. Pol. A 2018, 133(4), 959–964. https://doi.org/10.12693/APhysPolA.133.959
15. Reshmi, C.P.; Ramesh, A.R.; Suresh, A.; Jaiswal-Nagar, D. Magnetic, magnetocaloric and optical properties of nano $Gd_3Ga_5O_{12}$garnet synthesized by citrate sol-gel method. Int. J. Nano Dimens. 2025, 16, 190–201.
16. Luchechko, A.; Kostyk, L.; Varvarenko, S.; Tsvetkova, O.; Kravets, O. Green-Emitting $Gd_3Ga_5O_{12}$:Tb^{3+} Nanoparticles Phosphor: Synthesis, Structure, and Luminescence. Nanoscale Res. Lett. 2017, 12, 263.
17. Jovanić, B.; Bettinelli, M.; Radenković, B.; Despotović-Zrakić, M.; Bogdanović, Z. Optical spectroscopy of nanocrystalline $Gd_3Ga_5O_{12}$ doped with Eu3+ and high pressures. Mater. Chem. Phys. 2012, 132, 273–277.
18. Baillard, A.; Douissard, P.-A.; Loiko, P.; Martin, T.; Mathieu, E.; Camy, P. Terbium-doped gadolinium garnet thin films grown by liquid phase epitaxy for scintillation detectors. RSC Adv. 2025, 15, 20560–20568.
19. Wollesen, L.; Douissard, P.-A.; Pauwels, K.; Baillard, A.; Loiko, P.; Brasse, G.; Mathieu, J.; Simeth, S.J.; Kratz, M.; Dujardin, C.; et al. Microstructured growth by liquid phase epitaxy of scintillating $Gd_3Ga_5O_{12}$(GGG) doped with Eu3+. J. Alloys Compd.2025, 1010, 177267.
20. Wang, K.; Xu, J.; Murakami, H.; Yamahara, H.; Seki, M.; Tabata, H.; Tonouchi, M. Terahertz Time-Domain Spectroscopy of Substituted Gadolinium Gallium Garnet. Condens. Matter 2025, 10, 1. https://doi.org/10.3390/condmat10010001
21. Li, J.; Yousaf, M.; Ahmed, J.; Bibi, B.; Noor, A.; Alhokbany, N.; Sajid, M.; Nazar, A.; Shah, M.A.K.Y.; Guo, X.; Ding, X.; Mushtaq, N.; Lu, Y. $Gd_3Ga_5O_{12}$: A wide bandgap semiconductor electrolyte for ceramic fuel cells, effective at temperatures below 500 C. J. Rare Earths 2025, 43, 2248–2256.
22. Elzbieciak-Piecka, K.; Sójka, M.; Tian, F.; Li, J.; Zych, E.; Marciniak, L. The comparison of the thermometric performance of optical ceramics, microcrystals and nanocrystals of Cr3+-doped $Gd_3Ga_5O_{12}$ garnets. J. Alloys Compd. 2023, 963, 171284.
23. Shimoyama, N.; Kodama, S.; Bartosiewicz, K.; Fujiwara, C.; Yanase, I.; Takeda, H. Modification of Photoluminescence Wavelength and Decay Constant of Cr:$Gd_3Ga_5O_{12}$ Substituted by Ca/Si Cation Pair. J. Ceram. Soc. Jpn. 2024, 132(7), 364–368. https://doi.org/10.2109/jcersj2.23216
24. Kitaura, M.; Zen, H.; Watanabe, S.; Masai, H.; Kamada, K.; Kim, K.J.; Ueda, J. Relationship between Ce^{3+} $5d_1$ Level, Conduction-Band Bottom, and Shallow Electron Trap Level in $Gd_3Ga_5O_{12}$:Ce and $Gd_3Al_1Ga_4O_{12}$:Ce Crystals Studied via Pump–Probe Absorption Spectroscopy. Opt. Mater. X 2025, 25, 100398.
25. Petrenko, O.A.; Balakrishnan, G.; Paul, D.McK.; Yethiraj, M.; McIntyre, G.J.; Wills, A.S. Field Induced Magnetic Order in the Frustrated Magnet Gadolinium Gallium Garnet. J. Phys. Conf. Ser. 2009, 145, 012026. https://doi.org/10.1088/1742-6596/145/1/012026
26. Deen, P.P.; Florea, O.; Lhotel, E.; Jacobsen, H. Updating the Phase Diagram of the Archetypal Frustrated Magnet $Gd_3Ga_5O_{12}$. Phys. Rev. B 2015, 91, 014419. https://doi.org/10.1103/PhysRevB.91.014419

 doi:10.20944/preprints202510.2192.v1

27. Sackville Hamilton, A.C.; Lampronti, G.I.; Rowley, S.E.; Dutton, S.E. Enhancement of the Magnetocaloric Effect Driven by Changes in the Crystal Structure of Al-Doped GGG, $Gd_3Ga_{5-x}Al_xO_{12}$ ($0 \le x \le 5$). J. Phys. Condens. Matter 2014, 26(11), 116001. https://doi.org/10.1088/0953-8984/26/11/116001
28. Jin, X.; Zhao, J.; Gao, L.; Ma, H.; Oimod, H.; Zhu, H.; Li, Q.; Su, T.; Zhu, H.; Tegus, O.; Zhao, J. Influence of High-Pressure Heat Treatment on Magnetocaloric Effects and Magnetic Phase Transition in Single Crystal $Gd_3Ga_5O_{12}$. J. Rare Earths 2024, 42(11), 2112–2118. https://doi.org/10.1016/j.jre.2024.01.003
29. Chukalkin, Y.G.; Shtirts, V.R. Radiation Amorphization and Recovery of Crystal Structure in $Gd_3Ga_5O_{12}$ Single Crystals. Phys. Status Solidi A 1994, 144(1), 9–14. https://doi.org/10.1002/pssa.2211440102
30. Mironova-Ulmane, N.; Sildos, I.; Vasil'chenko, E.; Chikvaidze, G.; Skvortsova, V.; Kareiva, A.; Muñoz-Santiuste, J.E.; Pareja, R.; Elsts, E.; Popov, A.I. Optical Absorption and Raman Studies of Neutron-Irradiated $Gd_3Ga_5O_{12}$ Single Crystals. Nucl. Instrum. Methods Phys. Res. B 2018, 435, 306–312.
31. Potera, P.; Matkovskii, A.; Sugak, D.; Grigorjeva, L.; Millers, D.; Pankratov, V. Transient Color Centers in GGG Crystals. Radiat. Eff. Defects Solids 2002, 157(6–12), 709–713. https://doi.org/10.1080/10420150215740
32. Potera, P.; Ubizskii, S.; Sugak, D.; Schwartz, K. Induced Absorption in Gadolinium Gallium Garnet Irradiated by High-Energy ^{235}U Ions. Acta Phys. Pol. A 2010, 117, 181–183. https://doi.org/10.12693/APhysPolA.117.181
33. Karipbayev, Z.T.; Kumarbekov, K.; Manika, I.; Dauletbekova, A.; Kozловskiy, A.L.; Sugak, D.; Ubizskii, S.B.; Akilbekov, A.; Suchikova, Y.; Popov, A.I. Optical, Structural, and Mechanical Properties of $Gd_3Ga_5O_{12}$ Single Crystals Irradiated with $84Kr^+$ Ions. Phys. Status Solidi B 2022, 259(8), 2100415.
34. Meftah, A.; Costantini, J.M.; Khalfaoui, N.; Boudjadar, S.; Stoquert, J.P.; Studer, F.; Toulemonde, M. Experimental Determination of Track Cross-Section in $Gd_3Ga_5O_{12}$ and Comparison to the Inelastic Thermal Spike Model Applied to Several Materials. Nucl. Instrum. Methods Phys. Res. B 2005, 237(3–4), 563–574. https://doi.org/10.1016/j.nimb.2005.02.025
35. Toulemonde, M.; Meftah, A.; Costantini, J.M.; Schwartz, K.; Trautmann, C. Out-of-Plane Swelling of Gadolinium Gallium Garnet Induced by Swift Heavy Ions. Nucl. Instrum. Methods Phys. Res. B 1998, 146(1–4), 426–430. https://doi.org/10.1016/S0168-583X(98)00518-7
36. Meftah, A.; Assmann, W.; Khalfaoui, N.; Stoquert, J.P.; Studer, F.; Toulemonde, M.; Trautmann, C.; Voss, K.-O. Electronic Sputtering of $Gd_3Ga_5O_{12}$ and $Y_3Fe_5O_{12}$ Garnets: Yield, Stoichiometry and Comparison to Track Formation. Nucl. Instrum. Methods Phys. Res. B 2011, 269(9), 955–958. https://doi.org/10.1016/j.nimb.2010.12.083
37. Costantini, J.-M.; et al. Swift Heavy Ion-Beam Induced Amorphization and Recrystallization of Yttrium Iron Garnet. J. Phys.: Condens. Matter 2015, 27, 496001.
38. Costantini, J.-M.; Miro, S.; Lelong, G.; Guillaumet, M.; Toulemonde, M. Damage Induced in Garnets by Heavy-Ion Irradiations: A Study by Optical Spectroscopies. Philos. Mag. 2018, 98(4), 312–328. https://doi.org/10.1080/14786435.2017.1403659
39. Ozaki, N.; Nellis, W.J.; Mashimo, T.; Ramzan, M.; Ahuja, R.; Kaewmaraya, T.; Kimura, T.; Knudson, M.; Miyanishi, K.; Sakawa, Y.; Sano, T.; Kodama, R. Dynamic Compression of Dense Oxide ($Gd_3Ga_5O_{12}$) from 0.4 to 2.6 TPa: Universal Hugoniot of Fluid Metals. Sci. Rep. 2016, 6, 26000. https://doi.org/10.1038/srep26000
40. Khanin, V.M.; Rodnyi, P.A.; Wieczorek, H.; Ronda, C.R. Electron Traps in Gd3Ga3Al2O12:Ce Garnets Doped with Rare-Earth Ions. Tech. Phys. Lett. 2017, 43, 439–442.
41. Lisiecki, R.; Komar, J.; Macalik, B.; Strzęp, A.; Berkowski, M.; Ryba-Romanowski, W. Exploring the Impact of Structure-Sensitive Factors on Luminescence and Absorption of Trivalent Rare Earth Embedded in Disordered Crystal Structures of $Gd_3Ga_5O_{12}$–$Gd_3Al_5O_{12}$ and Lu_2SiO_5–Gd_2SiO_5 Solid Solution Crystals. Low Temp. Phys. 2023, 49, 310–315. https://doi.org/10.1063/10.0017241
42. Aralbayeva, G.M.; Manika, I.; Karipbayev, Zh.; Suchikova, Y.; Kovachov, S.; Sugak, D.; Popov, A.I. Micromechanical Properties of $Gd_3Ga_5O_{12}$ Crystals Irradiated with Swift Heavy Ions. J. Nano-Electron. Phys. 2023, 15(5), 05020. https://doi.org/10.21272/jnep.15(5).05020
43. Zorenko, Y.; Zorenko, T.; Voznyak, T.; Mandowski, A.; Xia, Q.; Batentschuk, M.; Friedrich, J. Luminescence of F^+ and F centers in Al_2O_3-Y_2O_3 oxide compounds. IOP Conf. Ser. Mater. Sci. Eng. 2010, 15, 012060.

 doi:10.20944/preprints202510.2192.v1

44. Babin, V.; Laguta, V.V.; Maaroos, A.; Makhov, A.; Nikl, M.; Zazubovich, S. Luminescence of F^+-type centers in undoped $Lu_3Al_5O_{12}$ single crystals. Phys. Status Solidi B 2011, 248, 845–852. https://doi.org/10.1002/pssb.201046245
45. Varney, C.R.; Selim, F.A. Color centers in YAG. AIMS Mater. Sci. 2015, 2, 560–572. https://doi.org/10.3934/matersci.2015.4.560
46. Pankratova, V.; Skuratov, V.A.; Buzanov, O.A.; Mololkin, A.A.; Kozlova, A.P.; Kotlov, A.; Popov, A.I.; Pankratov, V. Radiation effects in $Gd_3(Al,Ga)_5O_{12}:Ce^{3+}$ single crystals induced by swift heavy ions. Opt. Mater. X 2022, 16, 100217. https://doi.org/10.1016/j.omx.2022.100217
47. Pankratova, V.; Butikova, J.; Kotlov, A.; Popov, A.I.; Pankratov, V. Influence of swift heavy ions irradiation on optical and luminescence properties of $Y_3Al_5O_{12}$ single crystals. Opt. Mater. X 2024, 23, 100341. https://doi.org/10.1016/j.omx.2024.100341
48. Maji, S.B.; Vanetsev, A.; Mändar, H.; Nagirnyi, V.; Chernenko, K.; Kirm, M. Investigation of Luminescence Properties of Hydrothermally Synthesized Pr^{3+} Doped $BaLuF_5$ Nanoparticles under Excitation by VUV Photons. Opt. Mater. 2024, 154, 115781.
49. Krutyak, N.; Nagirnyi, V.; Romet, I.; Deyneko, D.; Spassky, D. Energy Transfer Processes in NASICON-Type Phosphates under Synchrotron Radiation Excitation. Symmetry 2023, 15, 749.
50. Spassky, D.; Voznyak-Levushkina, V.; Arapova, A.; Zadneprovski, B.; Chernenko, K.; Nagirnyi, V. Enhancement of Light Output in ScxY1−xPO4:Eu3+ Solid Solutions. Symmetry 2020, 12, 946.
51. Romet, I.; Tichy-Rács, É.; Lengyel, K.; Feldbach, E.; Kovács, L.; Corradi, G.; Chernenko, K.; Kirm, M.; Spassky, D.; Nagirnyi, V. Interconfigurational d–f Luminescence of Pr^{3+} Ions in Praseodymium Doped $Li_6Y(BO_3)_3$ Single Crystals. J. Luminescence 2024, 265, 120216.
52. Bartosiewicz, K.; Szysiak, A.; Tomala, R.; Gołębiewski, P.; Węglarz, H.; Nagirnyi, V.; Kirm, M.; Romet, I.; Buryi, M.; Jary, V.; et al. Energy-Transfer Processes in Nonstoichiometric and Stoichiometric Er3+, Ho3+, Nd3+, Pr3+, and Cr3+-Codoped Ce:YAG Transparent Ceramics: Toward High-Power and Warm-White Laser Diodes and LEDs. Phys. Rev. Appl. 2023, 20, 014047.
53. Gundacker, S.; Pots, R. H.; Nepomnyashchikh, A.; Radzhabov, E.; Shendrik, R.; Omelkov, S.; Kirm, M.; Acerbi, F.; Capasso, M.; Paternoster, G.; Mazzi, A.; Gola, A.; Chen, J.; Auffray, E. Vacuum Ultraviolet Silicon Photomultipliers Applied to BaF_2 Cross Luminescence Detection for High Rate Ultrafast Timing Applications. Phys. Med. Biol. 2021, 66 (11), 114002.
54. Saaring, J.; Feldbach, E.; Nagirnyi, V.; Omelkov, S.; Vanetsev, A.; Kirm, M. Ultrafast Radiative Relaxation Processes in Multication Cross Luminescence Materials. IEEE Trans. Nucl. Sci. 2020, 67 (6), 1009–1013.
55. Smortsova, Y.; Chukova, O.; Kirm, M.; Nagirnyi, V.; Pankratov, V.; Kataev, A.; Kotlov, A. The P66 time-resolved VUV spectroscopy beamline at PETRA III storage ring of DESY. J. Synchrotron Rad. 2025, 32. https://doi.org/10.1107/S1600577525007568
56. Andriichuk, V.A.; Volzhenskaya, L.G.; Zakharko, Ya.M.; Zorenko, Yu.V. Influence of structure defects upon the luminescence and thermostimulated effects in Gd3Ga5O12 crystals. J. Appl. Spectrosc. 1987, 47, 902–905. https://doi.org/10.1007/BF00659432
57. Randoshkin, V.V.; Vasil'eva, N.V.; Kolobanov, V.N.; Mikhailin, V.V.; Petrovnin, N.N.; Spasskii, D.A.; Sysoev, N.N. Effect of Gd_2O_3 concentration in Bi-containing high-temperature solutions on the luminescence of epitaxial $Gd_3Ga_5O_{12}$ films. Inorg. Mater. 2009, 45, 418–422.